Geophysical Journal International

Geophys. J. Int. (2012) **189,** 400–413 doi: 10.1111/j.1365-246X.2012.05351.x

Fortnightly Earth rotation, ocean tides and mantle anelasticity

Richard D. Ray[1] and Gary D. Egbert[2]

[1]*NASA Goddard Space Flight Center, Greenbelt, MD, USA. E-mail: richard.ray@nasa.gov*
[2]*College of Oceanic & Atmospheric Sciences, Oregon State University, Corvallis, OR, USA*

Accepted 2011 December 16. Received 2011 December 16; in original form 2011 May 9

SUMMARY

This study of the fortnightly Mf tide comprises three main topics: (1) a new determination of the fortnightly component of polar motion and length of day (LOD) from a multidecade time-series of observed space-geodetic data; (2) the use of the polar motion determination as one constraint in the development of a hydrodynamic ocean model of the Mf tide and (3) the use of these results to place new constraints on mantle anelasticity at the Mf tidal period. Our model of the Mf ocean tide assimilates more than 14 years of altimeter data from the Topex/Poseidon and Jason-1 satellites. Because the Mf altimetric signal-to-noise ratio is very small, it is critical that altimeter data not be overweighted. The polar motion data, plus tide-gauge data and independent altimeter data, give useful additional information, with only the polar motion putting constraints on tidal current velocities. The resulting ocean-tide model, plus the dominant elastic body tide, leaves a small residual in observed LOD caused by mantle anelasticity. The inferred effective tidal Q of the anelastic body tide is 90 and is in line with a ω^{α} frequency dependence with α in the range 0.2–0.3.

Key words: Earth rotation variations; Tides and planetary waves; Mantle processes.

1 INTRODUCTION

The near-fortnightly tide Mf, of period 13.66 d, is the largest of the zonally symmetric, long-period tides. Like all the long-period lunar tides, it may be thought of as a time-varying modulation of the Earth's permanent tide M_0. In the case of Mf, the modulation arises from the twice monthly excursion of the moon off the Earth's equator. The Mf time dependence is $\cos 2s$, where s is the mean longitude of the moon relative to the equinox.

At the Earth's surface, the Mf tidal potential is given by (Cartwright & Tayler 1971)

$$\Phi(\theta, t) = \sqrt{(5/16\pi)}\,(1 - 3\cos^2\theta)\,V_0 \cos 2s, \qquad (1)$$

where θ is colatitude and the amplitude V_0 is 0.65258 $\mathrm{m^2\,s^{-2}}$ (Table A1). The zonal symmetry of (1) induces a body tide that modulates the Earth's flattening, producing relatively large variations in length of day (LOD), with amplitude of order 0.4 ms.

To the extent that the Earth's response to the potential (1) is homogeneous there can be no Mf excitation of polar motion. The Earth's response, however, is not perfectly homogeneous, the largest inhomogeneity in this case being caused by the ocean. On theoretical grounds, one therefore expects that the Mf ocean tide induces a small variation in polar motion at 13.66 d. The first observational evidence of this was reported by Chao (1994) and Gross *et al.* (1996). The most complete analysis to date is by Gross (2009). The signal-to-noise ratio is small. We are motivated to re-examine the topic by some technical analysis details and also by the availability of newly released, consistent models of non-tidal angular momentum corrections (Dobslaw *et al.* 2010). These topics are addressed in Section 2.

One potentially important application of a refined estimate of fortnightly polar motion is that it provides a globally integrated constraint on models of the fortnightly ocean tide. This application may seem surprising in an age of satellite altimetry, in which determinations of all tides, including Mf (Egbert & Ray 2003), have markedly grown ever more accurate (e.g. Le Provost 2001). Yet while tidal elevations are well constrained by the near-global altimeter data, there are hardly any useful constraints on global tidal currents. For barotropic models of the short-period tides the lack of accurate tidal current measurements, while unfortunate, may not be critical; recent models, constrained only by altimetry, agree well with precise acoustic-tomographic measurements of currents (e.g. Dushaw *et al.* 1997; Ray 2001). The situation with long-period tides is quite different. Because of their low frequencies (relative to the sidereal frequency), long-period tides tend to be dominated by vorticity modes that are not well constrained by elevation measurements. Global angular momentum may therefore be a valuable model constraint. In Section 4, we develop a series of Mf ocean-tide solutions by assimilating over 14 years of Topex/Poseidon (T/P) and Jason-1 data into a global barotropic model, and we consider what constraints are imposed by the polar motion data.

An important application of a refined model of the fortnightly ocean tide is, in turn, that it provides a crucial correction when inferring mantle anelasticity from measurements of LOD. Tidal variations in LOD are one of the few mechanisms for probing the solid Earth at frequencies outside the seismic band, but the

ocean-tide and elastic body-tide effects on LOD dominate the anelastic effect. Estimates of fortnightly variations in LOD have existed for some time (e.g. Guinot 1970; Yoder *et al.* 1981; Hefty & Capitaine 1990; Robertson *et al.* 1994; Chao *et al.* 1995). We update and compare these estimates in Section 3. Implications regarding anelastic effects in the Earth's body tide are explored in Section 5.

In each section, we arrive at new estimates of some fundamental quantity related to the Mf tide. All quoted uncertainties throughout this paper correspond to one standard error.

2 FORTNIGHTLY POLAR MOTION

This section concentrates on the determination of 13.66-d term in the Earth's polar motion.

Throughout this section, we routinely convert back and forth between polar motion and polar motion excitation. The former is denoted by the complex number $p = p_1 + ip_2$, where p_1 and p_2 mark the location of the celestial ephemeris pole with respect to a body-fixed rotating frame, with p_1 the distance along the Greenwich meridian and p_2 along 90°E, and similarly for excitation $\chi = \chi_1 + i\chi_2$. For motions significantly longer than a day, p and χ are related by (e.g. Gross 2007)

$$p(t) + \frac{i}{\sigma_c}\frac{dp(t)}{dt} = \chi(t), \tag{2}$$

where σ_c is the complex frequency of the Chandler Wobble, which we take as $2\pi f_c(1 + i/2Q_c)$ where f_c is 1 cycle per 434 d and Q_c is 50 (Furuya & Chao 1996). The frequency-domain analogue of (2) is

$$\tilde{p}(\omega)\left(1 - \frac{\omega}{\sigma_c}\right) = \tilde{\chi}(\omega). \tag{3}$$

In practice, one must relax (3) at high frequencies to avoid undue noise magnification; a well-behaved digital filter is given by Wilson (1985). At the frequency ω of the Mf tide, the quantity in parentheses in (3) is very roughly 31, so a quick rule of thumb for converting the Mf excitation magnitude in mas to polar motion magnitude in μas is to multiply χ by 30.

2.1 Polar motion data

The polar motion data used in this study are the SPACE2008 time-series produced by Ratcliff & Gross (2010) from various space-geodetic Earth orientation measurements. The method employs a specially designed Kalman filter (Gross *et al.* 1998) to combine the disparate types of measurements and to produce a time-series with daily sampling interval; see also Morabito *et al.* (1988) and Gross (2000). The time-series extends from 1976 until middle 2009.

Fig. 1 shows the estimated standard errors in the daily x-component of polar motion. There is a clear and impressive error reduction over the course of the space-geodetic series, with errors dropping below 1 mas after 1983 and below 0.1 mas after about 1993. The present-day noise floor is roughly 0.04 mas in both x and y-components.

The degree of smoothing performed by the Kalman filter depends on the accuracy and sampling interval of the original space-geodetic data (Morabito *et al.* 1988). The filter effect and its possible attenuation of signal in certain frequency bands is most clearly brought out by comparing the spectrum of polar motion excitation over different time intervals. Such comparison is shown in Fig. 2. For the frequency band that includes the Mf tide (frequency 26.74 cpy),

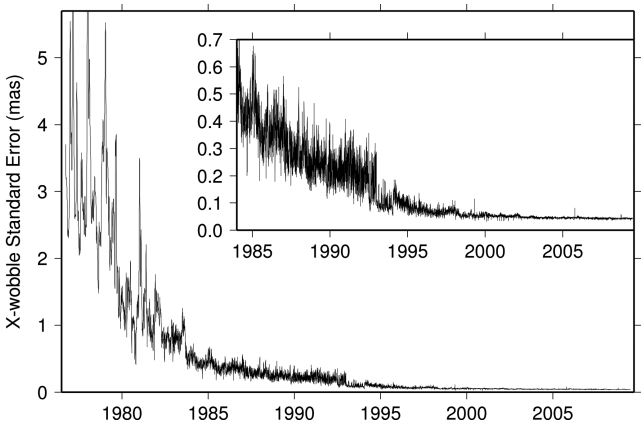

Figure 1. Standard errors in the SPACE2008 daily estimates of the p_1 component of polar motion, after Ratcliff & Gross (2010). The p_2 component is similar.

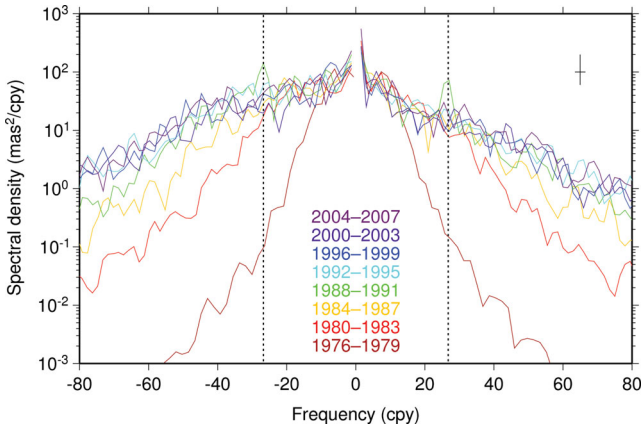

Figure 2. Spectra of SPACE2008 (Ratcliff & Gross 2010) polar motion excitation χ during successive 4-yr intervals. Negative frequencies refer to retrograde polar motion; positive to prograde. Vertical dotted lines denote the frequencies of the prograde and retrograde Mf tide. Older data from the SPACE2008 time-series are evidently strongly smoothed at high frequencies by the Kalman filter used to generate the data. Data after 1992 rely on daily space-geodetic polar motion measurements and are evidently minimally smoothed. Data between 1988 and 1991 are dampened at high frequencies but are apparently adequate at the Mf frequencies. Data before 1988 are suspect at the Mf frequencies.

all SPACE2008 data before 1988 are evidently prone to signal attenuation, severely so for the oldest data. The period 1988–1991 is marginal in this regard—its dampening appears to occur just above the Mf frequency—yet it is also the time period that displays the most conspicuous peak at Mf, possibly owing to the enhanced tide that occurred around 1988 from the Mf nodal modulation (see Fig. A1). All data after 1992 appear about equally smoothed at all frequencies, presumably owing to the routine availability of daily polar motion measurements after 1991 August. Based on Fig. 2, we are led to discard the polar motion data older than 1988 for any attempts at extracting the Mf tidal signal. [Incidentally, the C04 Earth rotation time-series described by Gambis (2004), which is available from the International Earth Rotation and Reference Systems Service (IERS), is also filtered in a way quite similar to that shown in Fig. 2.]

2.2 Correction for non-tidal effects

Because of the relatively small Mf signal, it is crucial to remove from the polar motion data as many non-tidal contributions as possible. As Ponte *et al.* (1998) and Gross *et al.* (2003) have shown, a large percentage of the non-tidal polar motion variance can be explained, and partially removed, by numerical models of the atmosphere and ocean. In this work, we experimented with two different sources for the required models; the following discussion applies equally to our LOD analysis in Section 3 later.

2.2.1 National Center for Environmental Prediction (NCEP)–Estimating the Circulation and Climate of the Ocean (ECCO) models

One of our selected set of models is consistent with those recently used by Gross (2009) for the same purpose. The effect of atmospheric angular momentum (AAM) is determined from the Reanalysis solutions of the NCEP and the National Center for Atmospheric Research (NCAR)—see Kalnay *et al.* (1996) for a discussion of the reanalysis products and their accuracies. The implied AAM estimates are readily available in the form of excitation functions from the IERS Special Bureau for Atmospheres (Salstein *et al.* 1993; Zhou *et al.* 2006). The component of AAM arising from relative motion is accounted for by analysed winds from the surface to the 10 hPa level; AAM from inertia is accounted for by barometric surface pressures, with an assumed isostatic inverted-barometer response over the oceans. At the period of the Mf tide, an isostatic ocean response to pressure loading appears to be a fairly accurate picture (Wunsch 1972; Ponte 1992), at least for the dominate wavenumbers associated with barometric surface pressure; at the gravest wavenumbers, such as those of the Mf tide itself, there is a small, but very clear, dynamic response (Egbert & Ray 2003), which is also evident in Fig. 5 later.

The corresponding oceanic angular momentum (OAM) was obtained from the IERS Special Bureau for the Oceans and is based on products of the ECCO consortium (Stammer *et al.* 2002). Two model time-series outputs were used here, both from the ECCO centre at the Jet Propulsion Laboratory and both based on the numerical circulation model of Marshall *et al.* (1997), which was forced by 12-hourly NCEP reanalysis winds and daily buoyancy fluxes (but not by pressure loading, which is thus consistent with our use of an inverted barometer for the AAM correction). The two ECCO runs are denoted c20010701 and kf066a2, for which OAM were computed only for the periods 1980–2002 and 1993–2008, respectively. The calculation of OAM for this ocean model is discussed in detail by Gross *et al.* (2003). The model did not assimilate oceanographic data nor was it forced by the gravitational tidal potential, so it is therefore properly non-tidal as required for present use.

We spliced together the two ECCO OAM series by using a weighted average over their period of overlap (after deleting the final 100 d of c20010701, which appear anomalous). The lack of pre-1980 data is of no concern because of limitations in the polar motion data themselves, as noted earlier. Our Earth rotation data after 2008 were retained without OAM corrections.

2.2.2 European Centre for Medium-Range Weather Forecasting (ECMWF)–GeoForschungsZentrum (GFZ) models

A second set of models employed here is based on work at the GFZ in Potsdam (Dobslaw *et al.* 2010). Models of the atmosphere, ocean and continental hydrosphere have been developed in a consistent fashion, each influencing or compensating the other to ensure consistent fluxes (e.g. of freshwater) and global mass conservation. The atmospheric component is one of several analysis or reanalysis products of the ECMWF. For the time-period of interest, here, we are able to use almost exclusively the ERA-Interim reanalysis (Simmons *et al.* 2006). Relative to earlier reanalyses widely available, ERA-Interim benefits from improved model physics, more sophisticated assimilation methods and improved resolution. Especially important for χ_3 angular momentum, wind data are provided up to the 0.1 hPa level.

The ocean and hydrosphere components of the GFZ model are supplied by the Ocean Model for Circulation and Tides (OMCT) and the Land Surface Discharge Model (LSDM) (Dill 2009), respectively. OMCT is forced by ECMWF winds, surface pressures and other relevant fluxes, and therefore no inverted barometer assumption need be adopted when computing the AAM. For further details of the models, see Dobslaw *et al.* (2010).

2.2.3 Model comparison

We have employed both sets of angular momentum corrections with the SPACE2008 time-series. Because we are primarily interested here in the long-period tidal band, we have computed the residual variance in the (10–70 cpy) frequency band for the period 1988–2009, after estimating and removing the tidal peaks. Table 1 lists these variances for all three components of angular momentum excitation. The first row is for no corrections, and subsequent rows show the effects of correcting for AAM, AAM+OAM, and finally the GFZ corrections.

It is evident that the GFZ corrections yield the lowest variances in the residual series. The reduction in variance of χ_3 is especially marked. Given the importance of atmospheric winds to the fluctuations of χ_3, we surmise that the more modern ERA-Interim product is responsible for this improvement. Because of the lower variances with the GFZ corrections, our preferred tidal solutions throughout this paper will be based on these, and other corrections are used only to examine sensitivity to these corrections.

The effect of the GFZ-based angular momentum corrections on the polar motion excitation spectrum is shown in Fig. 3. The importance of these corrections for isolating the Mf peaks from background noise is clearly evident in this figure. Note that before tidal analysis the data have also been high-pass filtered to remove the relatively large non-tidal energy evident in Fig. 3 at low frequencies.

2.3 Polar motion tidal estimates

The amplitudes and phases of the Mf tide were estimated from the corrected and filtered polar motion excitation data available over the

Table 1. Integrated residual variance of SPACE2008 in tidal band (10–70 cpy) after removal of models for atmospheric, oceanic and hydrologic angular momentum.

Source	AAM corr.	OAM corr.	HAM corr.	χ_1 (μas^2)	χ_2 (μas^2)	χ_3 (μs^2)
–	none	none	none	378	777	6240
IERS	NCEP	none	none	153	284	1087
IERS	NCEP	ECCO	none	94	197	873
GFZ	ECMWF	OMCT	LSDM	92	146	549

Notes: NCEP denotes Reanalysis-1.
ECMWF denotes primarily ERA-Interim reanalysis.

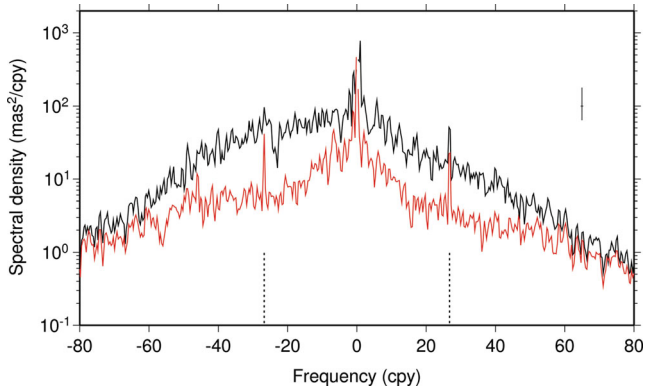

Figure 3. Spectrum of polar motion excitation before (black) and after (red) removal of non-tidal effects based on the GFZ models (Dobslaw *et al.* 2010) of atmospheric, oceanic and hydrologic angular momentum. Dotted vertical lines denote frequencies corresponding to the Mf tide. The polar motion Mf peaks are clearly more pronounced after adjustment.

time span 1988–2009. Some discussion of the method and estimated uncertainties is warranted.

Given the large variation in polar motion measurement error evident in Fig. 1, one might presume that weighted least squares should be employed for tidal estimation. This, however, is not the case, because the estimation of the Mf tidal parameters is limited by the noise of unmodelled (or mismodelled) non-tidal polar motion, not by the inherent measurement errors of polar motion. If measurement error is even roughly white, then a measurement error of, say, 0.1 mas, which is characteristic of post-1993 data, generates a noise spectrum of order

$$(0.1\ \text{mas})^2 \text{per } 183\ \text{cpy} \sim 10^{-4}\ \text{mas}^2\ \text{cpy}^{-1} \sim 10^2\ \mu\text{as}^2\ \text{cpy}^{-1},$$

which at the Mf frequency is equivalent to a noise spectrum in χ of order 10^{-1} mas^2 cpy^{-1}, between one and two orders of magnitude smaller than the observed spectrum around Mf. Similarly, the poorer 1985 measurement error corresponds to a white-noise floor of order 1 mas^2 cpy^{-1} in excitation, which is still considerably larger than the noise levels near Mf for the entire corrected SPACE2008 time-series (red curve in Fig. 3). We conclude that sources other than measurement error limits the delineation of the Mf peaks. Lacking other criteria, we therefore weighted the entire 1988–2009 time span of data equally in the least-squares tidal estimation.

As developed more fully in the Appendix, the Mf tidal constituent undergoes a relatively large (of order 40 per cent) modulation in amplitude, induced mainly by the regression of the moon's orbital node. Although this can be accounted for by independently estimating tidal parameters for the several spectral lines comprising Mf, such a course is not recommended when noise sources are large, which is here the case. We therefore estimate a single amplitude and phase for Mf, with nodal variation modelled by the classical f, u parameters as given in the Appendix. This implies a constant tidal admittance across the small band of frequencies comprising Table A1, which is eminently reasonable. It is true that in a few isolated cases fortnightly tides in shallow waters can violate the smooth-admittance assumption because of non-linear interactions between the diurnal O_1 and K_1 tides (the difference in their two frequencies is identical to the frequency of Mf), but these localized interactions do not appear to affect the global integral for polar motion (see later).

In addition to the Mf constituent, we estimated simultaneously tidal parameters for the MSm, Mm, MSf, Mt, and Mq constituents, for general noise reduction and correlation monitoring. The standard errors of these other tides are rather large relative to their amplitudes and they are not discussed further in this paper.

The standard errors of Mf have been estimated from the least-squares covariance, scaled by the spectral density of the time-series residuals near the Mf frequency. These standard errors have been checked in two ways: (1) Three false tides surrounding Mf have been simultaneously estimated and the rms of their in-phase and quadrature χ components is found to be 0.30 mas, which is consistent with our stated Mf standard errors. (2) The time-series has been partitioned into yearly segments, each subjected to tidal analysis, and the resulting scatter in the yearly Mf estimates is also found to be consistent with the stated Mf errors.

The least-squares estimates are given in Table 2 in terms of both excitation χ and polar motion p. The phase conventions used for the latter follow Munk & MacDonald (1960, eq. 6.7.5), defined by writing

$$p(t) = A^+ \mathrm{e}^{\mathrm{i}(\omega t + \alpha^+)} + A^- \mathrm{e}^{-\mathrm{i}(\omega t - \alpha^-)},$$

where $\omega t = 2s$.

The Mf standard error in χ_1 tends to be smaller than in χ_2, evidently because the overall variance in the χ_2 residual time-series is greater; when converted to prograde and retrograde polar motion the standard errors in each component are comparable—about 10 μas for the GFZ-corrected data.

The first line in Table 2 is our primary solution; the other lines summarize various sensitivity tests. Of these tests, the one with the largest effect on Mf is that made without correcting for the OAM. In that case, the least-squares residuals are considerably larger, which is reflected in the larger standard errors. The largest discrepancy appears to be in the amplitude of χ_2, but its larger standard error is consistent with this discrepancy.

It is of interest to compare these polar motion estimates with similar recent results obtained by Gross (2009), who used slightly different methods on a space-geodetic time-series equivalent to our IERS-corrected data, for the period 1980–2006. Gross obtained: $(A^+, \alpha^+) = (69, 254^\circ)$ and $(A^-, \alpha^-) = (89, 40^\circ)$ with standard errors of about 3 μas. Our standard errors are about three or four times larger, which we are inclined to argue are more realistic in light of the above-mentioned tests. Owing to our larger uncertainties, our estimates and Gross's are consistent, although both of his amplitudes are smaller than ours, possibly owing to his use of the pre-1988 data (note lower pre-1988 amplitudes shown in his fig. 2).

Table 2. Fortnightly polar motion estimates from space-geodetic data, 1988–2009.

	χ_1		χ_2		Prograde PM		Retrograde PM	
AAM/OAM	A, mas	G	A, mas	G	A^+, μas	α^+	A^-, μas	α^-
GFZ	2.94 ± 0.31	$359^\circ \pm 6^\circ$	4.83 ± 0.34	$337^\circ \pm 4^\circ$	76 ± 10	$257^\circ \pm 7^\circ$	99 ± 10	$43^\circ \pm 5^\circ$
IERS	2.92 ± 0.31	$352^\circ \pm 6^\circ$	4.71 ± 0.45	$334^\circ \pm 6^\circ$	76 ± 13	$261^\circ \pm 9^\circ$	96 ± 13	$38^\circ \pm 7^\circ$
IERS-A	2.85 ± 0.46	$350^\circ \pm 9^\circ$	5.38 ± 0.60	$339^\circ \pm 6^\circ$	91 ± 17	$261^\circ \pm 10^\circ$	100 ± 17	$44^\circ \pm 9^\circ$

Notes: IERS-A denotes IERS AAM only (no OAM).
Amplitude A and Greenwich phase lag G as in Appendix.

Table 3. Fortnightly Mf rotation rate estimates from space-geodetic data, 1985–2009.

AAM/OAM	$\Delta\Lambda$		ΔUT		Response coefficient	
	A, μs	G	A, μs	G	$\lvert\kappa\rvert$	$\arg\kappa$
GFZ	358.0 ± 0.6	$3.53^\circ \pm 0.09^\circ$	778.4 ± 1.3	$273.53^\circ \pm 0.09^\circ$	0.3131 ± 0.0005	$-3.53^\circ \pm 0.09^\circ$
IERS	359.2 ± 0.9	$3.63^\circ \pm 0.13^\circ$	780.9 ± 2.0	$273.63^\circ \pm 0.13^\circ$	0.3141 ± 0.0008	$-3.63^\circ \pm 0.13^\circ$
IERS-A	358.7 ± 1.1	$3.77^\circ \pm 0.16^\circ$	779.9 ± 2.4	$273.77^\circ \pm 0.16^\circ$	0.3137 ± 0.0010	$-3.77^\circ \pm 0.16^\circ$

Note: Amplitude A and Greenwich phase lag G as in Appendix.

As an aside, some readers may be interested in a test of the constant-admittance assumption for the lines within Mf. We therefore computed a least-squares solution for a set of completely independent spectral lines. The large Mf nodal line, with Doodson number (0 2 0 0 1 0), obtained (1.28 ± 0.31 mas, $339^\circ \pm 14^\circ$) for χ_1, and (1.99 ± 0.33 mas, $343^\circ \pm 9^\circ$) for χ_2. Predicted constant-admittance estimates for that line are (1.22 ± 0.14 mas, $359^\circ \pm 6^\circ$) for χ_1, and (2.00 ± 0.15 mas, $337^\circ \pm 4^\circ$) for χ_2. The admittances at the two Mf lines are therefore in agreement, although the phases of χ_1 differ by about 1.4 times the standard error.

3 FORTNIGHTLY VARIATIONS IN LOD

Unlike polar motion, where the signal of the Mf tide is fairly subtle and difficult to extract from background noise, the Earth's rotation rate exhibits an extraordinarily large Mf signal, first detected more than 50 years ago. The signal is dominated by large changes in the moment of inertia stemming from the Earth's body tide.

Tidal perturbations in rotation rate may be variously described in terms of excess LOD $\Delta\Lambda$, variations in Universal Time ΔUT1 relative to international atomic time TAI, or as a generalized response coefficient κ (Agnew & Farrell 1978). For any variation, the first two are related by

$$\Delta\mathrm{UT} = -\Lambda_0^{-1} \int \Delta\Lambda \, \mathrm{d}t,$$

where Λ_0 is the nominal LOD (86 400 s). Taking now a general tidal variation of frequency ω and converting to complex notation, we have the following relationships between the three LOD variables:

$$\Delta\mathrm{UT} = \mathrm{i}(\omega\Lambda_0)^{-1}\Delta\Lambda$$

and

$$\Delta\Lambda = \kappa^* \Lambda_0 \frac{R^3}{3GC} \left(\frac{5}{\pi}\right)^{1/2} V_0,$$

where R is the mean earth radius, G the Newtonian constant, C the polar moment of inertia and V_0 is the potential amplitude as in eq. (1) with normalization (following Agnew & Farrell) as in Munk & Cartwright (1966).

As with polar motion, we used the SPACE2008 time-series of Ratcliff & Gross (2010) for estimating the Mf variation in LOD. Computed spectra of 4-yr segments of the SPACE2008 LOD series (not shown) are similar to the results for polar motion as presented in Fig. 2, except that the data in the 1984–1987 window appear satisfactory and only the pre-1984 data are obviously oversmoothed in the Mf band. Our Mf rotation rate estimates are therefore based on the series from 1985 to 2009.

AAM and OAM (and potentially hydrologic angular momentum) corrections were applied to the LOD data, analogous to the corrections described earlier for the polar motion data. Each correction results in reduced variance in the residuals (which is also implied from the detailed discussion of Gross *et al.* 2004), and hence in reduced Mf standard errors.

The estimated Mf parameters for rotation rate are tabulated in Table 3. As in Table 2, the preferred solution is listed first; the other lines summarize various sensitivity tests, including the effect of the correction for non-tidal ocean angular momentum. The latter has a much smaller influence on LOD than was seen for polar motion, which is not unexpected given the large LOD signals arising from other sources. However, its quoted uncertainties are considerably larger, obviously reflecting the larger residual variances noted in Table 1.

There is an important difference to note that occurs in the Ratcliff–Gross processing of LOD data compared with their polar motion data. In processing of the LOD measurements, they used a prior model of the long-period tides to remove the dominant tidal effects, then applied their Kalman filter to the residuals and added back the prior model. This is standard procedure for handling deterministic signals and minimizing the effects of smoothing. However, to the extent that the Kalman filter may have removed energy near the Mf frequency, the final series could be more or less simply the prior model of Mf. Whereas the LOD spectra (corresponding to Fig. 2) suggest that the Kalman filter may not have removed energy near the Mf band (after 1984), we were sufficiently concerned by this possibility that we obtained an independent LOD series from colleagues at Goddard Space Flight Center (GSFC; David Gordan, personal communication, 2011), which is based completely on Very Long Baseline Interferometry (VLBI) measurements and used no prior model of long-period tides in its derivation. Specifically, we obtained the series gsf2010a.eops, which in fact was one of the fundamental geodetic time-series used as input to the SPACE2008 processing. The GSFC series comprises daily averages of LOD with an uneven sampling corresponding to the availability of VLBI networks; on average, there is a measurement two or three times per week. We adjusted these data with the IERS AAM and OAM corrections, rejected about 3 per cent of the data as anomalous, and estimated tidal coefficients. For $\Delta\Lambda$, we obtained 359.1 ± 2.7 μs amplitude and $4.1^\circ \pm 0.4^\circ$ phase lag. The standard errors are large relative to our primary solution from SPACE2008, owing to the reduced number of data. The results are nonetheless quite consistent, suggesting that the use of a prior when deriving SPACE2008 does not unduly influence the final Mf signal.

Table 4 compares some previously published Mf LOD estimates. The majority of these date from the mid-1990s, and they should be less precise than ours simply owing to the much extended time-series now at our disposal. All estimates shown in Table 4 use corrections for AAM, although the corrections may derive from different meteorological centres. The Englich *et al.* result is a recent VLBI estimate which agrees well with ours in amplitude (again suggesting that the SPACE2008 prior did no significant harm). The result from Benjamin *et al.* (2006) is essentially identical to our methods used for line 2 of Table 3 except that we now have a longer time-series.

Given the stated uncertainties in Table 4, the various estimates of κ are not completely consistent, especially in phase. (Note that a 1° discrepancy in the phase of Mf corresponds very nearly to

Table 4. Selected published estimates of Mf response coefficient from observed rotation rates.

Authors	Time span	$\|\kappa\|$	$\arg\kappa$
Merriam (1984)	1978–1982	0.317 ± 0.013	$-5.8^\circ \pm 2.2^\circ$
McCarthy & Luzum (1993)	1984–1991	0.306 ± 0.001	$-1.38^\circ \pm 0.24^\circ$
Robertson *et al.* (1994)	1984–1993	0.3128 ± 0.0013	$-3.55^\circ \pm 0.24^\circ$
Chao *et al.* (1995)	1980–1992	0.3106 ± 0.0020	$-2.7^\circ \pm 0.4^\circ$
Dickman & Nam (1995)	1985–1993	0.306 ± 0.010	$-2.7^\circ \pm 0.7^\circ$
Benjamin *et al.* (2006)	1985–2003	0.3139 ± 0.0009	$-3.50^\circ \pm 0.18^\circ$
Englich *et al.* (2009)	1984–2008	0.3129 ± 0.0008	$-3.98^\circ \pm 0.15^\circ$
This paper	1985–2009	0.3131 ± 0.0005	$-3.53^\circ \pm 0.09^\circ$

1 hr in time.) Of the older tabulated estimates, our results agree most closely with those of Robertson *et al.* (1994). The early work of Merriam (1984), within its understandably large uncertainties owing to the shortness of his time-series, is also consistent.

4 GENERALIZED INVERSION FOR THE FORTNIGHTLY OCEAN TIDE

The goal of this section is to describe the development of a new numerical model of the Mf ocean tide and to examine whether the above polar motion determination adds any useful constraints in the modelling process. The new Mf model in turn is used in Section 5 to remove the ocean-tide component from the LOD data.

Our approach to forward and inverse ocean-tide modelling follows Egbert *et al.* (1994) and Egbert & Erofeeva (2002). Forward modelling provides a necessary prior for the inversion step, and it may well yield the only satisfactory solution if inadequate data are lacking for assimilation—such, in fact, is likely the case for all long-period tidal constituents other than Mf and perhaps Mm. This point provides sufficient motivation to improve the realism of forward models of long-period tides to the greatest extent possible. One of our early forward models of Mf appeared in the work of Egbert & Ray (2003), and a considerably improved version was used by Benjamin *et al.* (2006).

4.1 Forward modelling

We adopt a direct, frequency-domain, factorization approach to solving the linearized shallow-water equations Egbert & Erofeeva (2002). One particular factorization solution was checked with a non-linear, time stepping approach and was found to produce very similar results; this justifies use of the linear solver for most of our computations. The system was solved on a global 1/4° finite-difference grid. Inclusion of the Arctic Ocean, which is essential for models of long-period tides, was accomplished by using a rotated coordinate system with the north pole over Greenland. Forcing from self-attraction and crustal loading effects should normally be computed through an iterative procedure, with initial elevations fed into relevant integrals to recompute the forcing and the procedure iterated until convergence. Since all long-period tides are fairly close to equilibrium, however, it here suffices to use a single prior elevation model to compute these effects.

One outstanding question is the extent to which non-linear interactions of short-period tides affect the tidal angular momentum—see, in particular, the discussion by Cartwright (1997) concerning the MSf constituent. In the case of Mf, the relevant interactions are between the diurnal tides O_1 and K_1. As a test of the importance of this interaction, we used an efficient linearized modelling approach (Egbert *et al.* 2010) which employs accurate altimeter-based models of the two diurnal constituents to compute forcing at the Mf frequency. The shallow-water equations were then solved with the astronomical forcing for Mf alone and with the additional K_1–O_1 interaction added. The addition of the non-linear terms is found to have negligible impact on the global integrals of tidal angular momentum—the largest impact is in the prograde component of polar motion where the amplitude is affected by about 0.6 per cent. Much larger perturbations can result from different (and uncertain) parametrizations of tidal friction in the numerical model, as noted below.

4.2 Inverse modelling

A series of data assimilation experiments using T/P and Jason-1 satellite altimeter data were conducted with several goals in mind: (1) to provide an estimate of the likely magnitude of errors in polar motion and UT1 computed from a purely numerical forward, (2) to clarify how tightly the altimeter data should be fit in an inversion and (3) ultimately to obtain the best estimates of the Mf ocean tide's contribution to Earth rotation.

In the linearized approach employed here, the tidal solution is controlled essentially by two parameters: (1) f_v, a 'friction velocity' which linearizes the standard quadratic bottom friction dissipation with f_v replacing $|v|$ in $c_D|v|v/H$, where H is water depth and $c_D = 0.0025$ (Egbert & Erofeeva 2002), and (2) σ_e, a trade-off parameter used to scale the assumed data error covariance and thus to control the degree of fit to the altimeter data. Each parameter is limited to a certain range, either by physical arguments or by error-covariance arguments, but within these ranges there is some degree of flexibility. In our most recent work, we varied the strength of f_v both for the prior model and for the inversion; values of 0.3, 1, 3 and 10 m s^{-1} were tried. These apparently large values for f_v cover the range we have found appropriate for linear tide modelling. For Mf, we get the best agreement of the prior solution with validation data for $f_v = 1$ and the worst for $f_v = 0.3$. Our inversion experiments thus used only the three largest values of f_v.

The assimilated altimeter data consist of Mf harmonic constants deduced along satellite ground-tracks from 531 repeat cycles (each of 9.9 d duration) of T/P and Jason-1 altimetry. Before tidal analysis, considerable effort was expended to ensure consistency between the two satellite missions, including new satellite ephemerides computed in a consistent terrestrial reference frame and also employment of the most up-to-date radiometer calibrations (Beckley *et al.* 2004, 2010). In addition, and for consistency with the above rotation estimations, the altimetric heights have been corrected for non-tidal variability by using the ECCO kf066a2 modelling outputs. (We emphasize again that kf066a2 did not assimilate altimetry nor did it include gravitational tidal forces.)

The impact of varying the trade-off parameter and the different friction velocities is shown in Fig. 4 in terms of calculated polar motion (details later). For the inertia components (arising from ocean tidal heights) all levels of fit tried produce similar polar motion; for the prograde component, especially, all the inverse solutions differ significantly from the priors, which are already quite variable. For the motion components (arising from ocean tidal currents), there is larger scatter and a more continuous change as σ_e is reduced and the fit to the altimetry is improved. The primary impact of our uncertainty in how well data should be fit arises from the motion terms.

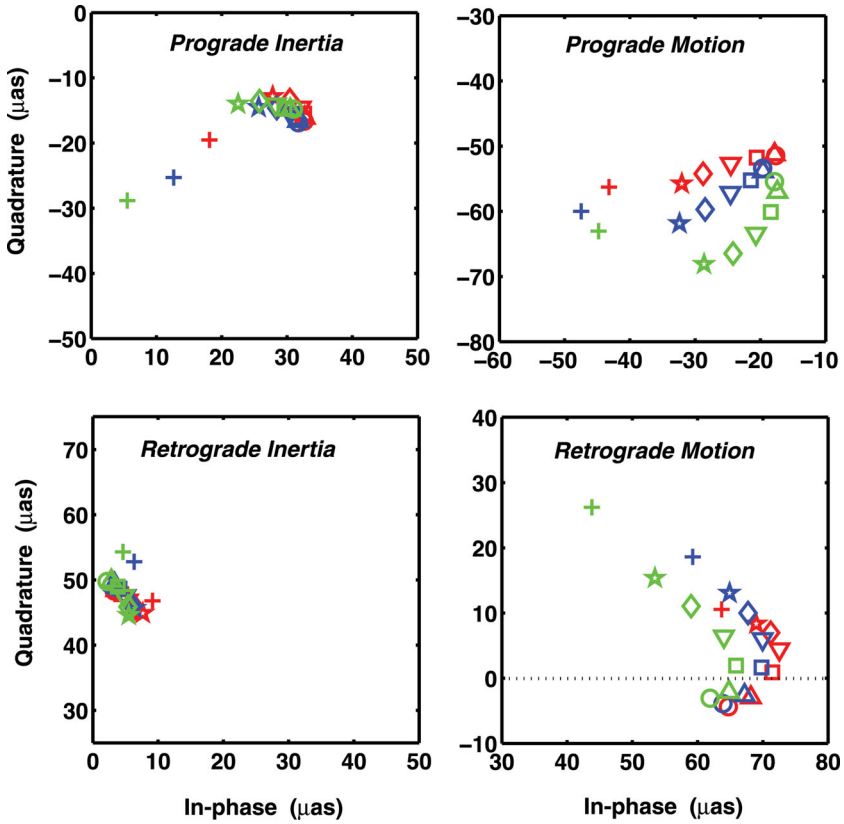

Figure 4. Inertia and relative motion terms for prograde and retrograde polar motion according to a large suite of ocean-tide inversions. The three colours of symbols correspond to different prior models, using different friction velocities, with red, blue and green corresponding to 1, 3 and 10 m s^{-1}, respectively. The plus symbols give polar motion for the three priors; other symbols correspond to increasingly better fit to altimeter data, with circles fitting most tightly.

The larger sensitivity of the motion terms is consistent with changes to the inverse solutions as σ_e is varied. Very subtle, and rather small scale, altimeter signals are fit when σ_e is small, resulting in very substantial increases in (small scale) currents, even while elevations are relatively unaffected; see Fig. 5 where inverse solutions for two values of σ_e are shown.

4.3 Comparisons with independent data

In this section, the ocean-tide solutions are compared with three types of independent data: altimetry, tide gauges and the above polar motion estimates. These critical tests allow us to delimit the free parameters of the inversion and to arrive at a preferred ocean-tide solution.

4.3.1 Comparisons with independent altimetry

Given the paucity of reliable Mf harmonic constants (but see later), we primarily used unassimilated altimeter data to calibrate the optimal level of data fit for the inverse solution. For this, we used along-track Mf harmonic constants calculated from 114 cycles (about 3 yr) of T/P altimetry data from its interleaved orbit; rms differences for inverse solutions computed for a range of values of σ_e, and with prior solutions computed with the three values of f_v are plotted in Fig. 6. The individual along-track harmonic constants are very noisy, and none of the inverse solutions explains a large fraction of the observed variance. Nonetheless, averaged over the global ocean, there is a very clear reduction in rms for all of the inverse solutions, with a minimum at $\sigma_e = 100$ or so—corresponding to fitting the altimeter data only weakly. Fig. 6 also suggests that the smallest value for friction velocity ($f_v = 1$) is the best choice. The Mf inverse solution corresponding to $f_v = 1$, $\sigma_e = 100$ is plotted in the right column of Fig. 5. Note that relaxing the fit further (i.e. taking $\sigma_e = 300$) increases the rms difference with the altimeter validation data only slightly.

4.3.2 Tide gauge comparison

To our knowledge, the best compilation of Mf harmonic constants derived from open-ocean tide gauges stems from some older work by Prof. Doug Luther, eventually published as appendix A of Miller *et al.* (1993). From his 24 stations—all small islands in the Pacific Ocean—we rejected any Mf estimate with standard error exceeding 3 mm and we rejected station Apia, noted by Luther as suspect because of an anomalously large MSf, suggestive of non-linear influences. This left 19 sets of Mf harmonic constants.

Statistics summarizing the observed differences between these island data and our $f_v = 1$ assimilation solutions are tabulated in Table 5. The variation among the solutions is small and is not statistically significant, at least according to a Snedecor test of the ratio of tabulated rms values. Nonetheless, we show the results because they are consistent with those seen in our above altimeter tests: The assimilation of altimetry results in a more accurate Mf solution than the hydrodynamic prior, so long as the altimetry is not overweighted. The trade-off parameter σ_e should be no less than about 100.

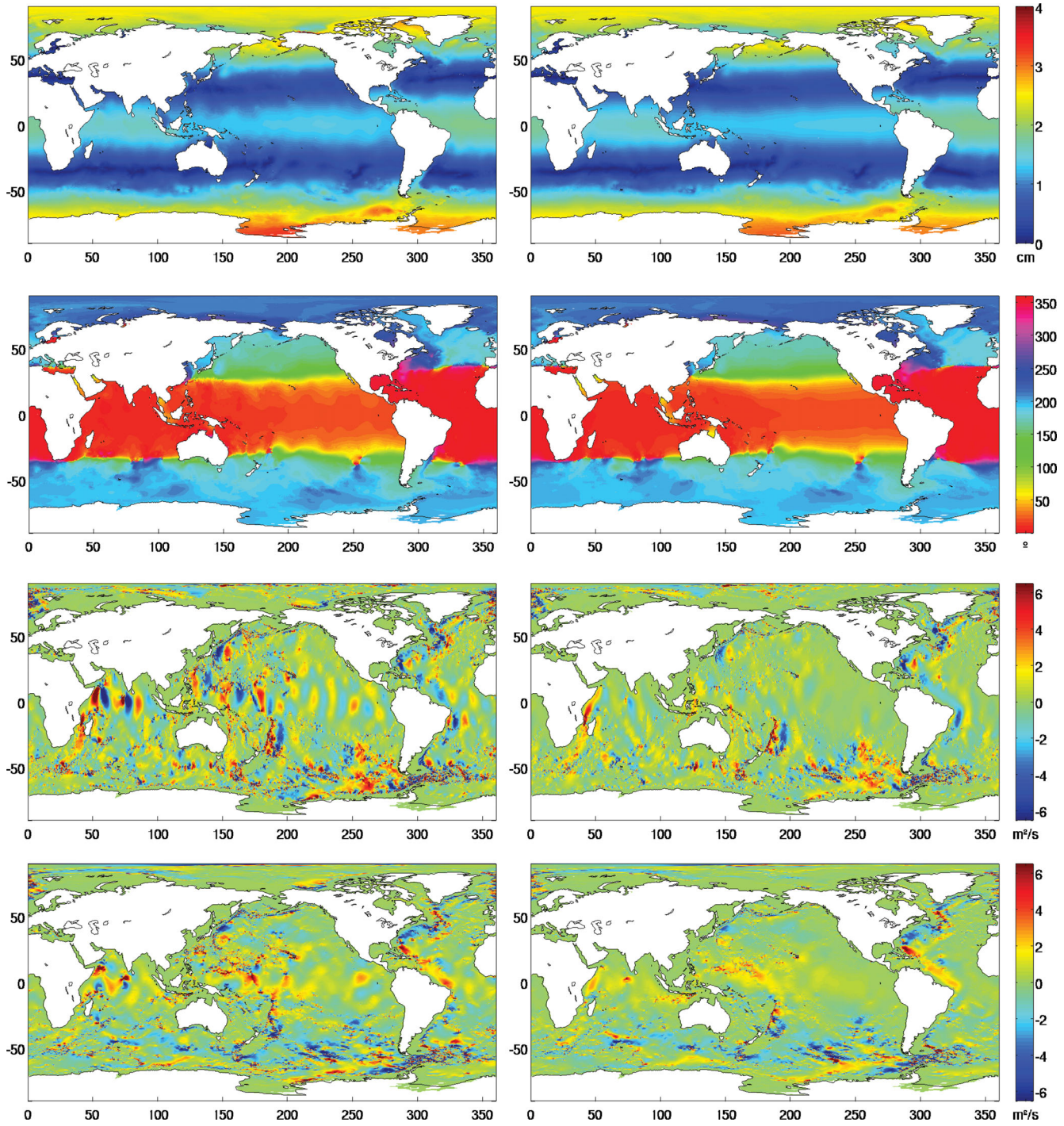

Figure 5. Inverse solutions of the Mf ocean tide, for two values of the trade-off parameter that controls fitting the altimeter data. Left column is better fitting ($\sigma_e = 1$), right column has relaxed data fit ($\sigma_e = 100$). Top to bottom: amplitude, phase lag, north–south and east–west volume transports (real parts only). Note the relatively large changes in currents associated with only very subtle elevation changes. The right column gives the preferred solution, as discussed in the text. The elevations clearly display some large-scale, non-equilibrium features, with the low-latitude Pacific tide being smaller and lagging the low-latitude Atlantic tide; for further details, see Egbert & Ray (2003).

4.3.3 Polar motion comparison

Mf polar motion has been computed from the elevations and current velocities for all our prior and inverse ocean-tide solutions. The calculation of polar motion from these data uses a generalization of (2) that accounts for the resonance near the nearly diurnal free wobble (e.g. Gross 1993), although that adjustment is very small for motion at the Mf period. The components of these computed polar motions stemming from either tidal heights or currents were shown earlier as Fig. 4. Ocean tidal heights and currents are seen to contribute about equally to polar motion.

The sum totals of polar motion are shown in Fig. 7, again for three different prior models and for a range of trade-off parameters. The circles in Fig. 7 correspond to the observed Mf polar motion,

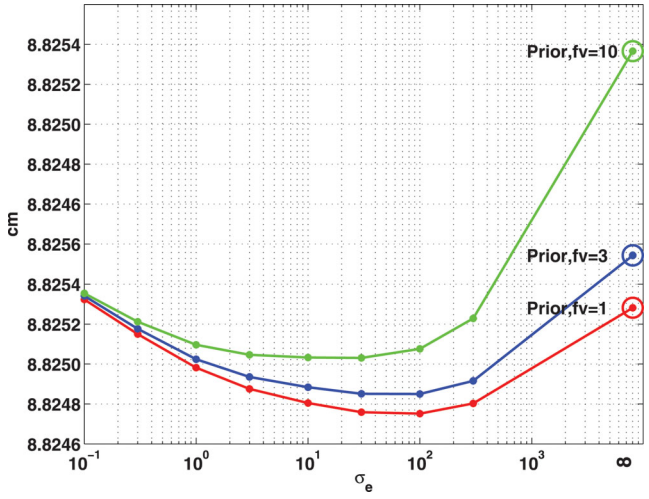

Figure 6. rms differences between various Mf ocean-tide assimilation solutions and an independent set of Mf solutions computed empirically from T/P altimeter data along its interleaved track. Colours denote different friction velocities, and σ_e is the trade-off parameter between fitting altimeter data versus the hydrodynamic model. Far right points correspond to prior models, before assimilation.

Table 5. Tide-gauge tests of weights for ocean-tide inversions.

σ_e	rms (mm)	MAD (mm)
∞	0.84	0.55
300	0.80	0.45
100	0.81	0.48
30	0.84	0.51
10	0.88	0.57

MAD, median absolute difference.
Note: $\sigma_e = \infty$ refers to prior (solution with no altimetry).

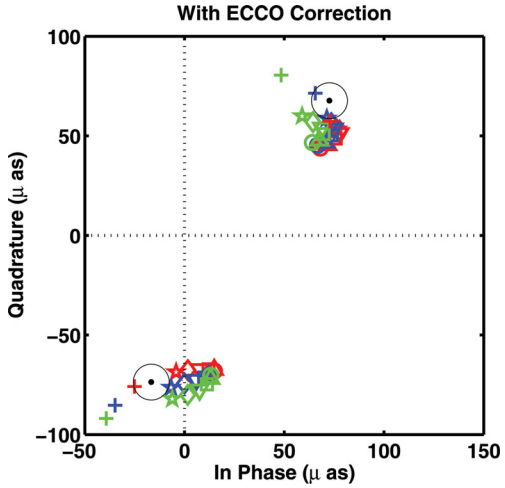

Figure 7. Total prograde (lower left cluster) and retrograde (upper right) polar motion computed from a suite of ocean-tide inversions, with three different priors and a range of trade-off parameters. Colours and symbols are as in Fig. 4. The large open circles are centred on our observed Mf polar motion (Table 2), with radius corresponding to one standard error. Our preferred ocean-tide solution is denoted by the red star.

according to the first line of Table 2. The results for the prior, purely numerical model are in reasonable agreement with the independent geodetic estimates. The best agreeing prior (red plus) is obtained with the $f_v = 1$ m s^{-1} friction velocity. Fitting the altimetry generally moves the computed polar motion towards, and then past, the geodetic estimates, with parameters for all priors converging to a common value.

Comparison with observed prograde polar motion suggests that inversions strongly fitting the altimeter data are not to be preferred, which is consistent with the other tests above. It also suggests that weakly fitting the altimetry is beneficial, especially if the prior model employed one of the larger values for friction. Overall, the best agreements in Fig. 7 are seen to be the red plus, the red star (both with $f_v = 1$) and the blue star, which all agree about equally with observed polar motion. Although polar motion provides our only test dependent on tidal current velocities, it is in the end consistent with the other tests on elevations alone.

4.4 Preferred ocean solution

The earlier tests suggest the preferred ocean-tide inversion is the one having the weakest fit to the altimeter data ($\sigma_e = 300$) and the smallest linear friction coefficient ($f_v = 1$). (This solution is denoted by the red star in the previous figures.) For reference, the computed Earth rotation parameters for this model are tabulated in Table 6. The conversion of tidal angular momentum to LOD here follows eq. (46) of Gross (2007), which depends on the adoption of a number of geophysical constants, notably the loading Love number k_2' and a parameter α_3 that scales k_2' to account for core decoupling. Owing to the high precision required for ΔUT in Section 5, it is important to establish its sensitivity to our adopted constants, including the possibility that k_2' has a small imaginary component. It appears that uncertainty in these constants leads to uncertainty in ΔUT of roughly 1 per cent. Coincidentally, the adopted constants used to compute polar motion (including the Chandler Wobble frequency) are of far less concern because of the fairly large scatter from our tidal inversions and because subsequent analysis below does not depend on these precise values.

According to Table 6, for LOD, the inertia terms of the Mf tide dominate; the relative angular momentum of the tidal currents contribute only about 10 per cent to the total variations. This is the opposite of short-period tides where the currents tend to dominate the axial angular momentum budget (Baader *et al.* 1983; Ray *et al.* 1994). The phase of the inertia term lags a purely equilibrium model by 16°, a not insignificant amount, which probably reflects the notable phase lag associated with the tidal elevations of the Pacific Ocean; see Fig. 5.

The ΔUT results for all our various tide inversions are shown in Fig. 8. The scatter in ΔUT gives useful information towards assigning a reasonable uncertainty to the ocean tide's contribution; note that our preferred tide solution is seen to fall in the middle of the scatter. The two low-friction priors (red and blue pluses) sit off to the side somewhat separated, but while these two priors give acceptable polar motion, our other tests suggest they are less accurate than the preferred solution. Defining the ocean-tide uncertainty in terms of the scatter of the better solutions shown in Fig. 8 could be overly optimistic, of course, if some unrecognized systematic error affects all solutions. We have endeavoured to eliminate such problems to the extent possible. For example, all solutions include the Arctic Ocean; failure to do so can easily result in UT errors of order 10 μs. We also account rigorously for tidal self-attraction and

Table 6. Earth rotation effects of the Mf ocean tide.

	Prograde PM		Retrograde PM		ΔΛ		ΔUT	
	A^+, μas	α^+	A^-, μas	α^-	Amp. (μs)	Phase	Amp. (μs)	Phase
Tidal heights	30.6	335.2°	45.5	80.3°	47.8	16.36°	103.9	286.36°
Tidal currents	64.3	240.1°	69.5	6.9°	5.0	84.25°	10.8	354.25°
Total	68.8	266.5°	93.3	34.8°	49.9	21.65°	108.5	291.65°

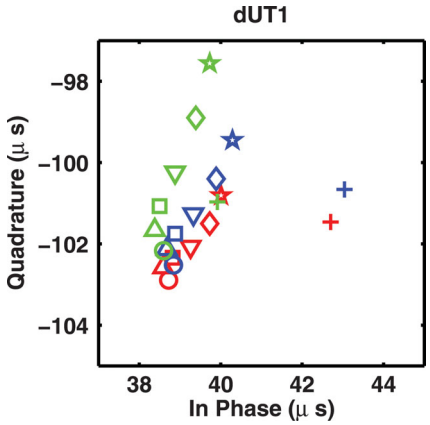

Figure 8. As in Fig. 7 but for ΔUT rotation rate variations. Our preferred ocean-tide inversion is denoted by the red star, which happens to sit near the middle of the shown cluster. For comparison, the Mf model of Kantha *et al.* 1998) is (48.5, −104.2) μs, and of Dickman (discussed by Dickman & Gross 2010) is (23, −107) μs.

use a fairly high-resolution global grid; both aspects are critical for physical realism (e.g. Arbic *et al.* 2004).

Based on the scatter in Fig. 8 and particularly in the spread between the solutions favoured by our various tests, our preferred UT ocean-tide components (in-phase and quadrature) are: 40.0 ± 2 and -100.8 ± 3 μs, respectively. The uncertainties cover the roughly 1 per cent uncertainty arising from various adopted geophysical constants noted earlier.

5 CONSTRAINTS ON MANTLE ANELASTICITY

We are finally in a position to bring together the various strands of this paper to form a consistent interpretation of fortnightly Earth rotation. The observational space-geodetic data, corrected via models for non-tidal angular momentum, yield fairly precise estimates of Mf LOD or ΔUT. The components of the Earth system that account for the Mf oscillations are laid out in Fig. 9. The elastic response of the body tide dominates, as is well known.

The residual in Fig. 9 may be attributed to several causes: the quoted uncertainties in the elastic body tide and/or ocean-tide contributions may be too optimistic; there may be residual coupling between the mantle and core; anelasticity in the body tide may modify the magnitude of the elastic tide and introduce a small phase lag. The latter effect is certainly expected (e.g. Wahr & Bergen 1986).

It has been realized since the early 1980s that the Earth's core is unlikely to participate in such rapid spin variations (Merriam 1980; Wahr *et al.* 1981; Yoder *et al.* 1981). Clearly, from Fig. 9, were the core and mantle fully coupled, the models would diverge from the observed ΔUT even though coupling would slightly reduce the ocean-tide effect through changes in the loading factor α_3 (Merriam 1982). Could there be some small residual coupling? Calculations based on viscous coupling (Wahr *et al.* 1981) and

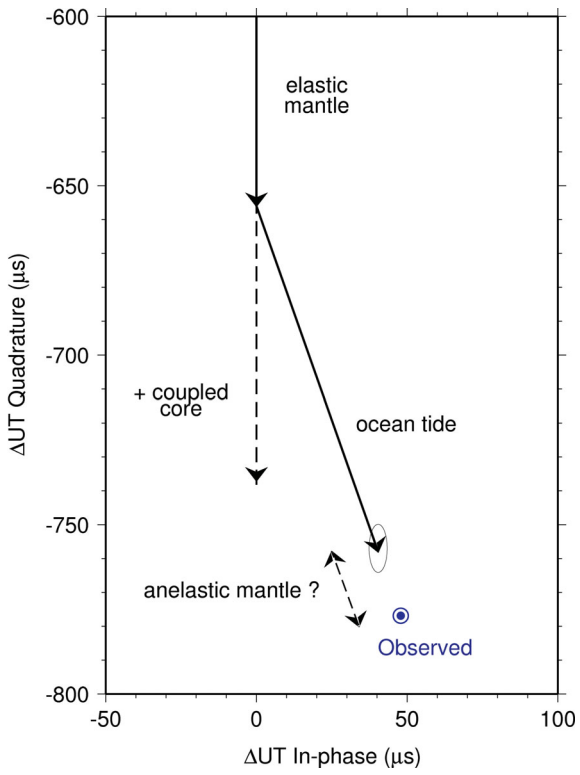

Figure 9. Decomposition of Mf variations in UT1 in terms of an elastic mantle, an ocean tide and an inferred mantle anelasticity. Observed value is shown by the blue dot. Error ellipse on the model sum represents the combined uncertainties of the elastic mantle and the ocean tide. Because UT1 represents an integration in time of ΔΛ, its in-phase ($\cos 2s$) and quadrature ($\sin 2s$) components are flipped relative to components of the tide-generating potential; the large component from the elastic response of the mantle, which dominates the figure, is thus in the quadrature component. The model vectors would be poorly aligned with the observed value if the core were not taken as decoupled from the mantle. Note the zoomed scale relative to figure origin.

topographic coupling (Wu & Wahr 1997) suggest extremely small contributions to ΔUT, but electromagnetic coupling (e.g. Koot *et al.* 2010) may not be so easily dismissed, partly owing to poorly known material properties near the core–mantle boundary. Nonetheless, for the following discussion, we follow most previous authors by assuming perfectly uncoupled core and mantle, allowing us to attribute the residual in Fig. 9 to mantle anelasticity.

The effect of a purely elastic mantle has been computed by several authors and they agree at about the 1 per cent level. Some are reviewed by Defraigne & Smits (1999). The differences arise primarily from differences in adopted earth models. We follow Benjamin *et al.* (2006) and adopt the value ΔUT = 656 μs based on the PREM earth model. Defraigne & Smits obtained 654 μs, whereas Wahr *et al.* (1981) obtained 663 μs based on the earlier 1066A earth model.

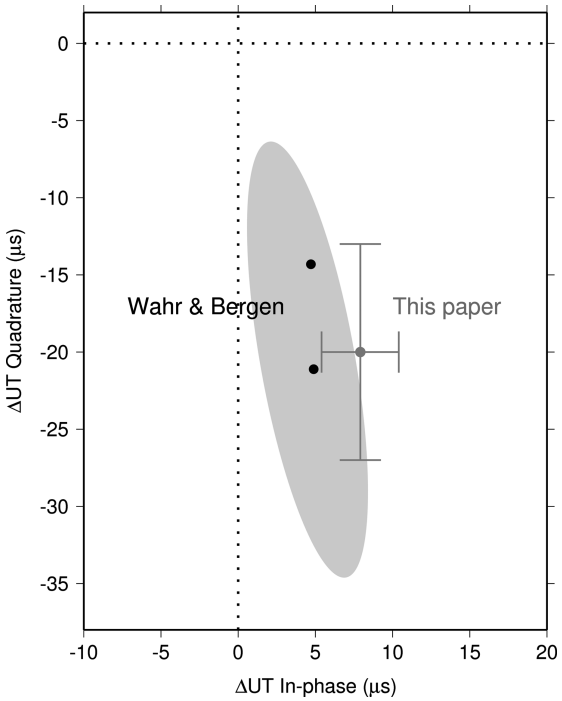

Figure 10. Contribution to ΔUT caused by anelasticity of the mantle as estimated in this paper (blue dot with 1σ error uncertainties). The lower black dot is 'Model B' and the upper is 'Model QMU' of Wahr & Bergen (1986); the grey shading depicts approximately the Wahr–Bergen upper and lower bounds.

Based on all the above estimates, the Mf ΔUT budget is as follows (in sine and cosine components, units of μs):

Observed	-776.9 ± 1.3	47.9 ± 1.3
Elastic body	-656 ± 6	0
Ocean tide	-100.8 ± 3	40.0 ± 2
Residual	-20 ± 7	7.9 ± 2.4

Fig. 10 compares this residual with theoretical estimates of the effect of mantle anelasticity calculated by Wahr & Bergen (1986). Their estimates rely on analysis of the mantle's specific dissipation Q^{-1} obtained by Smith & Dahlen (1981), and they also give upper and lower bounds, where the lower bound assumes the Q at the Mf period is the same as the Q at seismic periods and the upper bound assumes the Q at Mf is the same as the Chandler Wobble Q (based on a *ca.* 1986 estimate). Our results fall well within the Wahr–Bergen limits, although larger values for the component out-of-phase with the elastic tide appear to be preferred.

Defraigne & Smits (1999) also calculated the anelastic component in-phase with the elastic tide, and they obtained values between -15.6 and -19.7 μs, which agrees well with our -20 ± 7 μs.

For the Mf body tide as a whole, the above estimates imply a phase lag relative to the tidal potential of $0.67^\circ \pm 0.21^\circ$, for an effective tidal Q of about 90 with 1σ bounds of about 65–135. This Q falls between an estimated value of 280 for the M_2 tide (Ray *et al.* 2001) and a value of 50 for the Chandler Wobble (Furuya & Chao 1996), although the Chandler Wobble Q has a wide range of other published estimates, some higher than 90, which warrants re-examination and clarification.

It is of interest to place these Mf estimates into the context of the even larger range of frequencies analysed by Benjamin *et al.* (2006). To do this, we follow their lead and express the Earth's

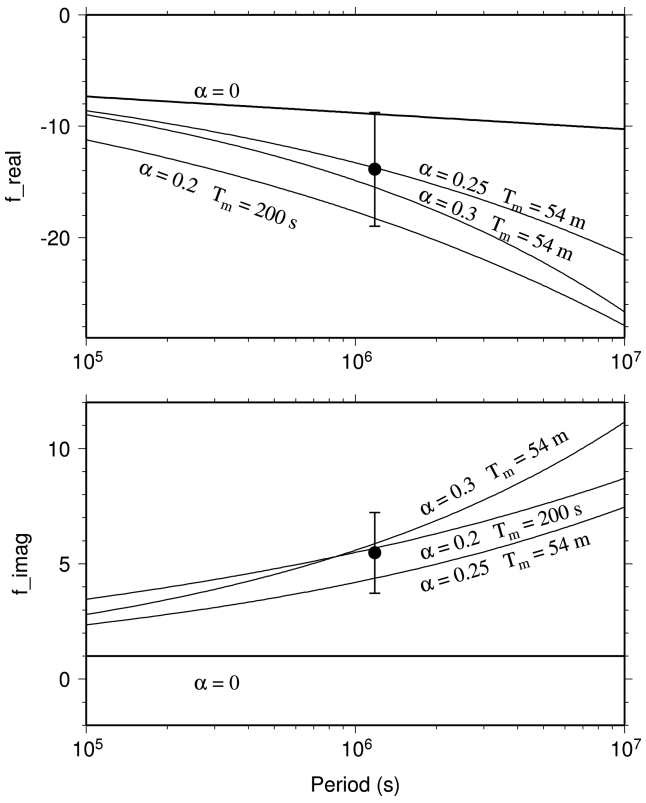

Figure 11. Observational estimates of (top panel) f_r and (bottom panel) f_i with analytical predictions for three anelastic models which intersect both error bars, following Benjamin *et al.* (2006).

shear modulus μ in the form

$$\mu(\omega) = \mu_0 + \frac{\mu_0}{Q_0}\,[f_r(\omega) + \mathrm{i}\, f_i(\omega),\,]$$

where μ_0 is the shear modulus at some reference frequency ω_0. This expression defines two functions, f_r and f_i, which represent the anelastic effects of dispersion and dissipation, respectively. Our estimates of the Mf ΔUT anelastic components correspond to the f_r, f_i shown in Fig. 11—see Benjamin *et al.* for details on how this correspondence is done. Also shown in Fig. 11 are several theoretical models of f_r, f_i based on different dependences of Q on frequency, all assumed to be in the simplified form

$$Q(\omega) = Q_0(\omega/\omega_0)^\alpha \qquad \omega < \omega_m,$$

where ω_m is some transition frequency marking the band above which Q is constant. Benjamin *et al.* examine a wide range of such models, over a large frequency interval and with transition periods $T_m = 1/\omega_m$ either 54 min or 200 s, but we show here in Fig. 11 only a few curves that intersect both error bars of our f_r, f_i estimates. Together, our estimates are seen to favour an α in the range 0.2–0.3. This result is consistent with the findings obtained by Benjamin *et al.* (2006) for T_m of 54 min. Their results for $T_m = 200$ s allows slightly smaller α, but it gives a poorer fit at the M_2 frequency.

It is perhaps surprising that the largest contributor to the formal uncertainties in the present Mf estimates now arises from the model of the elastic body tide. An uncertainty of ±6 μs is possibly pessimistic since it is primarily based on differences with some obsolete earth models, but we are not in a position at this point to clarify the issue. It would be of interest to examine more comprehensive models of the sort recently used by Latychev *et al.* (2009) to compute Earth-tide displacements.

6 CONCLUDING REMARKS

The LOD effects of mantle anelasticity are not only clearly detectable in these Mf tidal data (Fig. 9), but they are of a precision to begin to place valuable new constraints on anelastic models. This improved precision results from efforts on several fronts. Improved models of AAM and OAM (Dobslaw *et al.* 2010) have resulted in reduced non-tidal variance in the long-period tidal band, which allows better estimates of the observed LOD—compare the various uncertainties given in Table 3. Similarly, the LOD effects induced by ocean tides have been refined. This is the result of a large number of modelling improvements made over a number of years which have enhanced the physical realism of the numerical models—see, for example, discussions by Egbert *et al.* (2004) and Arbic *et al.* (2004), which are focused on the M_2 tide but which also apply to some extent to Mf. The ocean models for Mf have improved to the point where we find that the assimilation of altimeter data adjusts the numerical priors by only small amounts. Of course, this is partly the result of the very small signal-to-noise ratio in Mf sea level data; in contrast, assimilation of altimetry is still critical for producing accurate models of short-period tides.

The fact that altimetry must be downweighted in our Mf solutions does imply that its use may be even more marginal for other long-period constituents where signal-to-noise ratios are even smaller. For these cases, with the possible exception of Mm, results must rely upon purely numerical models. We are therefore encouraged by the closeness of our prior models to the observed polar motion, which does allow some inference about errors when extrapolating to other frequencies.

The present results for the effect of anelasticity on LOD are close to theoretical expectations (Wahr & Bergen 1986), with a slight preference towards larger values of the component out-of-phase with the elastic tide, thus hinting towards larger values of dissipation with an effective Q near 90. Uncertainties are nonetheless relatively large (Fig. 10). That the largest source of uncertainty in our analysis arises from the elastic response of the mantle suggests a rather obvious next step for improving these estimates.

ACKNOWLEDGMENTS

We thank John Wahr, Ben Chao, Richard Gross and Bruce Buffett for useful discussions. Lana Erofeeva provided essential help with the ocean-tide modelling. This work was funded by the U.S. National Aeronautics and Space Administration through the Ocean Surface Topography program and the Earth Surface and Interior program.

REFERENCES

Agnew, D.C. & Farrell, W.E., 1978. Self-consistent equilibrium tides, *Geophys. J. R. astr. Soc.,* **55,** 171–181.

Arbic, B.K., Garner, S.T., Hallberg, R.W. & Simmons, H.L., 2004. The accuracy of surface elevations in forward global barotropic and baroclinic tide models, *Deep-Sea Res. II,* **51,** 3069–3101.

Baader, H.-R., Brosche, P. & Hövel, W., 1983. Ocean tides and periodic variations of the earth's rotation, *Z. Geophys.,* **52,** 140–142.

Beckley, B.D., Zelensky, N.P., Luthcke, S.B. & Callahan, P.S., 2004. Towards a seamless transition from Topex/Poseidon to Jason-1, *Mar. Geod.,* **27,** 373–384.

Beckley, B.D., Zelensky, N.P., Holmes, S.A., Lemoine, F.G., Ray, R.D., Mitchum, G.T., Desai, S.D. & Brown, S.T., 2010. Assessment of the Jason-2 extension to the Topex/Poseidon, Jason-1 sea-surface height time-series for global mean sea level monitoring, *Mar. Geod.,* **33,** 447–471.

Benjamin, D., Wahr, J., Ray, R.D., Egbert, G.D. & Desai, S.D., 2006. Constraints on mantle anelasticity from geodetic observations, and implications for the J2 anomaly, *Geophys. J. Int.,* **165,** 3–16.

Cartwright, D.E., 1997. Some thoughts on the spring-neap cycle of tidal dissipation, *Progr. Oceanogr.,* **40,** 125–133.

Cartwright, D.E. & Tayler, R.J., 1971. New computations of the tide generating potential, *Geophys. J. R. astr. Soc.,* **23,** 45–74.

Chao, B.F., 1994. Zonal tidal signals in the Earth's polar motion, *EOS, Trans. Am. geophys. Un.,* **75,** 158.

Chao, B.F., Merriam, J.B. & Tamura, Y., 1995. Geophysical analysis of zonal tidal signals in length of day, *Geophys. J. Int.,* **122,** 765–775.

Defraigne, P. & Smits, I., 1999. Length of day variations due to zonal tides for an inelastic earth in non-hydrostatic equilibrium, *Geophys. J. Int.,* **139,** 563–572.

Dickman, S.R. & Gross, R.S., 2010. Rotational evaluation of a long-period spherical harmonic ocean tide model, *J. Geod.,* **84,** 457–464.

Dickman, S.R. & Nam, Y.S., 1995. Revised predictions of long-period ocean tide effects on Earth's rotation rate, *J. geophys. Res.,* **100,** 8233–8243.

Dill, R., 2009. Hydrological model LSDM for operational Earth rotation and gravity field variations, *Sci. Tech. Rep. 08/09,* Deutsches GeoForschungsZentrum, Potsdam.

Dobslaw, H., Dill, R., Grötzsch, A., Brzeziński, A. & Thomas, M., 2010. Seasonal polar motion excitation from numerical models of the atmosphere, ocean, and continental hydrosphere, *J. geophys. Res.,* **115,** B10406, doi:10.1029/2009JB007127.

Doodson, A.T. & Warburg, H.D., 1941. *Admiralty Manual of Tides,* HMSO, London.

Dushaw, B.D., Egbert, G.D., Worcester, P.F., Cornuelle, B.D., Howe, B.M. & Metzger, K., 1997. A Topex/Poseidon global ocean tidal model and barotropic tidal currents determined from long-range acoustic transmissions, *Prog. Oceanogr.,* **40,** 337–367.

Egbert, G.D. & Erofeeva, S.Y., 2002. Efficient inverse modeling of barotropic tides, *J. Atmos. Ocean. Technol.,* **19,** 183–204.

Egbert, G.D. & Ray, R.D., 2003. Deviation of long period tides from equilibrium: kinematics and geostrophy, *J. Phys. Oceanogr.,* **33,** 822–839.

Egbert, G.D., Bennett, A.F. & Foreman, M.G. G., 1994. Topex/Poseidon tides estimated using a global inverse model, *J. geophys. Res.,* **99,** 24 821–24 852.

Egbert, G.D., Ray, R.D. & Bills, B.G., 2004. Numerical modeling of the global semidiurnal tide in the present day and in the last glacial maximum, *J. geophys. Res.,* **109,** C03003, doi:10.1029/2003JC001973.

Egbert, G.D., Erofeeva, S.Y. & Ray, R.D., 2010. Assimilation of altimetry data for nonlinear shallow-water tides: Quarter diurnal tides of the Northwest European Shelf, *Cont. Shelf Res.,* **30,** 668–24 679.

Englich, S., Schuh, H. & Weber, R., 2009. Short-term tidal variations in UT1: compliance between modelling and observation, In *Proc. Intl. Astronom. Union 5,* p. 215.

Furuya, M. & Chao, B.F., 1996. Estimation of period and Q of the Chandler wobble, *Geophys. J. Int.,* **127,** 693–702.

Gambis, D., 2004. Monitoring Earth orientation using space-geodetic techniques: state-of-the-art and prospective, *J. Geod.,* **78,** 295–303.

Gross, R.S., 1993. The effect of ocean tides on the earth's rotation as predicted by the results of an ocean tide model, *Geophys. Res. Lett.,* **20,** 293–296, doi:10.1029/2002JB002143.

Gross, R.S., 2000. Combinations of Earth orientation measurements: SPACE97, COMB97, and POLE97, *J. Geod.,* **73,** 627–637.

Gross, R.S., 2007. Earth rotation variations: long period, in *Treatise on Geophysics, Vol. 3: Geodesy,* ch. 9, pp. 239–294, ed. Schubert, G., Elsevier, Amsterdam.

Gross, R.S., 2009. An improved empirical model for the effect of long-period ocean tides on polar motion, *J. Geod.,* **83,** 635–644.

Gross, R.S., Hamdan, K.H. & Boggs, D.H., 1996. Evidence for excitation of polar motion by fortnightly ocean tides, *Geophys. Res. Lett.,* **23,** 1809–1812.

Gross, R.S., Eubanks, T.M., Steppe, J.A., Freedman, A.P., Dickey, J.O. & Runge, T.F., 1998. A Kalman-filter-based approach to combining independent Earth orientation series, *J. Geod.,* **72,** 213–235.

Gross, R.S., Fukumori, I. & Menemenlis, D., 2003. Atmospheric and oceanic excitation of the Earth's wobbles during 1988–2000, *J. geophys. Res.,* **108**(B8), 2370, doi:10.1029/2003JB002432.

Gross, R.S., Fukumori, I., Menemenlis, D. & Gegout, P., 2004. Atmospheric and oceanic excitation of length-of-day variations during 1988–2000, *J. geophys. Res.,* **109,** B01406.

Guinot, B., 1970. Short-period terms in Universal Time, *Astron. Astrophys.,* **8,** 26–28.

Hartmann, T. & Wenzel, H.-G., 1995. The HW95 tidal potential catalogue, *Geophys. Res. Lett.,* **22,** 3553–3556.

Hefty, J. & Capitaine, N., 1990. The fortnightly and monthly zonal tides in the Earth's rotation from 1962 to 1988, *Geophys. J. Int.,* **103,** 219–231.

Kalnay, E. *et al.*, 1996. The NCEP/NCAR 40 year reanalysis project, *Bull. Am. Meteorol. Soc.,* **77,** 437–471.

Kantha, L.H., Stewart, J.S. & Desai, S.D., 1998. Long-period lunar fortnightly and monthly ocean tides, *J. geophys. Res.,* **103,** 12639–12647.

Koot, L., Dumberry, M., Rivoldini, A., deViron, O. & Dehant, V., 2010. Constraints on the coupling at the core-mantle and inner core boundaries inferred from nutation observations, *Geophys. J. Int.,* **182,** 1279–1294.

Latychev, K., Mitrovica, J.X., Ishii, M., Chan, N.-H. & Davis, J.L., 2009. Body tides on a 3-D elastic earth: toward a tidal tomography, *Earth planet. Sci. Lett.,* **277,** 86–90.

Le Provost, C., 2001. Ocean tides, in *Satellite Altimetry and Earth Sciences,* eds Fu, L.-L. & Cazenave, A., Academic Press, San Diego.

McCarthy, D.D. & Luzum, B.J., 1993. An analysis of tidal variations in the length of day, *Geophys. J. Int.,* **114,** 341–346.

Marshall, J., Adcroft, A., Hill, C., Perelman, L. & Helsey, C., 1997. A finite-volume, incompressible Navier-Stokes model for studies of the ocean on parallel computers, *J. geophys. Res.,* **102,** 5753–5766.

Merriam, J.B., 1980. Zonal tides and changes in length of day, *Geophys. J. R. astr. Soc.,* **62,** 551–561.

Merriam, J.B., 1982. A comparison of recent theoretical results on the short-period terms in length of day, *Geophys. J. R. astr. Soc.,* **69,** 837–840.

Merriam, J.B., 1984. Tidal terms in universal time: effects of zonal winds and mantle *Q, J. geophys. Res.,* **89,** 10 109–10 114.

Miller, A.J., Luther, D.S. & Hendershott, M.C., 1993. The fortnightly and monthly tides: Resonant Rossby waves or nearly equilibrium gravity waves?, *J. Phys. Oceanogr.,* **23,** 879–897.

Morabito, D.D., Eubanks, T.M. & Steppe, J.A., 1988. Kalman filtering of Earth orientation changes, in *The Earth's Rotation and Reference Frames for Geodesy and Geodynamics,* pp. 257–267, eds Babcock, A.K. & Wilkins, G.A., Reidel, Dordrecht.

Munk, W.H. & Cartwright, D.E., 1966. Tidal spectroscopy and prediction, *Phil. Trans. R. Soc. Lond. A,* **259,** 533–581.

Munk, W.H. & MacDonald, G.J.F., 1960. *The Rotation of the Earth,* Cambridge University Press, Cambridge.

Ponte, R.M., 1992. The sea level response of a stratified ocean to barometric pressure forcing, *J. Phys. Oceanogr.,* **22,** 109–113.

Ponte, R.M., Stammer, D. & Marshall, J.A., 1998. Oceanic signals in observed motions of the Earth's pole of rotation, *Nature,* **391,** 476–479.

Ray, R.D., 2001. Inversion of oceanic tidal currents from measured elevations, *J. Mar. Syst.,* **28,** 1–18.

Ray, R.D., Steinberg, D.J., Chao, B.F. & Cartwright, D.E., 1994. Diurnal and semidiurnal variations in the Earth's rotation rate induced by oceanic tides, *Science,* **264,** 830–832.

Ray, R.D., Eanes, R.J. & Lemoine, F.G., 2001. Constraints on energy dissipation in the earth's body tide from satellite tracking and altimetry, *Geophys. J. Int.,* **144,** 471–480.

Ratcliff, J.T. & Gross, R.S., 2010. Combinations of Earth orientation measurements: SPACE2008, COMB2008, and POLE2008, JPL Publ. 10-4, Jet Propulsion Laboratory, Pasadena, 27pp.

Robertson, D.S., Ray, J.R. & Carter, W.E., 1994. Tidal variations in UT1 observed with very long baseline interferometry, *J. geophys. Res.,* **99,** 621–636.

Salstein, D.A., Kann, D.M., Miller, A.J. & Rosen, R.D., 1993. The Subbureau for Atmospheric Angular Momentum of the International Earth Rotation Service: a meteorological data center with geodetic applications, *Bull. Am. Meteorol. Soc.,* **74,** 67–80.

Simmons, A., Uppala, S., Dee, D. & Kobayashi, S., 2006. ERA Interim: new ECMWF reanalysis products from 1989 onwards, *ECMWF Newsletter,* **110,** 25–35.

Smith, M.L. & Dahlen, F.A., 1981. The period and Q of the Chandler Wobble, *Geophys. J. R. astr. Soc.,* **64,** 223–282.

Stammer, D., Wunsch, C., Fukumori, I. & Marshall, J.A., 2002. State estimation in modern oceanographic research, *EOS, Trans. Am. geophys. Un.,* **83**(27), 289, 294–295.

Wahr, J.M. & Bergen, Z., 1986. The effects of mantle anelasticity on nutations, earth tides, and tidal variations in rotation rate, *Geophys. J. R. astr. Soc.,* **87,** 633–668.

Wahr, J.M., Sasao, T. & Smith, M.L., 1981. Effect of the fluid core on changes in the length of day due to long period tides, *Geophys. J. R. astr. Soc.,* **64,** 635–650.

Wilson, C.R., 1985. Discrete polar motion equations, *Geophys. J. R. astr. Soc.,* **80,** 551–554.

Wu, X. & Wahr, J.M., 1997. Effects of non-hydrostatic core-mantle boundary topography and core dynamics on Earth rotation, *Geophys. J. Int.,* **128,** 18–42.

Wunsch, C., 1972. Bermuda sea level in relation to tides, weather, and baroclinic fluctuations, *Rev. Geophys. Space Phys.,* **10,** 1–49.

Yoder, C.F., Williams, J.G. & Parke, M.E., 1981. Tidal variations of earth rotation, *J. geophys. Res.,* **86,** 881–891.

Zhou, Y.H., Salstein, D.A. & Chen, J.L., 2006. Revised atmospheric excitation function series related to earth variable rotation under consideration of surface topography, *J. geophys. Res.,* **111,** D12108, doi:10.1029/2005JD006608.

APPENDIX: SPECTRAL DEFINITION OF Mf

Recall that the classical definition of a tidal 'constituent' is a cluster of tidal spectral lines whose first three Doodson numbers are identical (Munk & Cartwright 1966). For the Mf tidal constituent, the first three Doodson numbers are (0 2 0). The largest such lines are listed in Table A1. The amplitudes are taken from the tables of Hartmann & Wenzel (1995) in a normalization consistent with eq. (1) and for times appropriate to the present era. Other lines within the Mf constituent are more than an order of magnitude smaller than those listed.

The two largest Mf lines differ in their fifth index by 1, and hence differ in frequency by 1 cycle in 18.6 yr. This is the dominant 'nodal modulation' of Mf, induced by the large variation in the moon's declination (from 18° to 28°) over the course of the 18.6-yr precession of the moon's orbit plane. This modulation also has a significant second harmonic. The fourth major line (0 2 0 −2 0 0) differs from the main Mf line by twice the lunar perigee frequency, or 1 cycle in 4.42 yr.

Table A1. Spectral lines of the Mf tidal constituent.

Doodson argument							
τ	s	h	p	N'	p'	ω (° h^{-1})	V_0 (m^2 s^{-2})
0	2	0	−2	0	0	1.088749	0.02825
0	2	0	0	0	0	1.098033	0.65258
0	2	0	0	1	0	1.100239	0.27058
0	2	0	0	2	0	1.102446	0.02531

Notes: Doodson numbers give integral coefficients in the tidal arguments for the following astronomical variables: τ, mean lunar time (in angular units); s, mean longitude of moon; h, mean longitude of sun; p, mean longitude of lunar perigee; N', negative of mean longitude N of lunar node; p', mean longitude of solar perigee.
For consistency with the Agnew–Farrell definition of κ, the Hartmann–Wenzel V_0 values have been scaled by $\sqrt{(4\pi)}$.

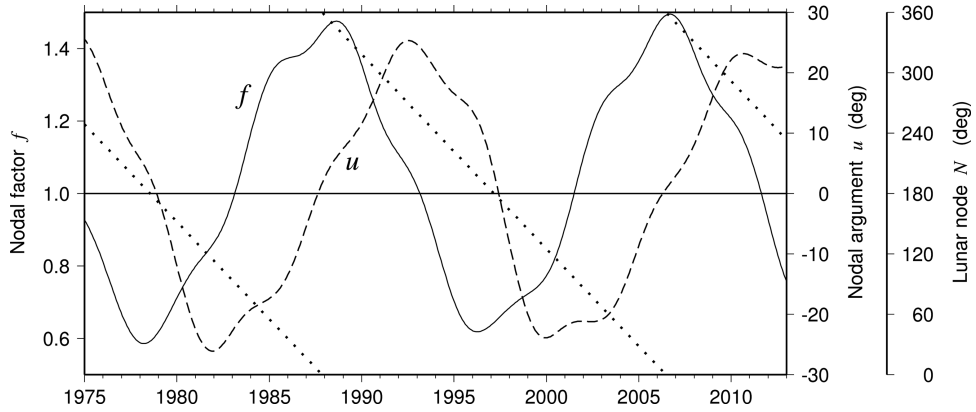

Figure A1. Nodal (and perigee) correction factors $f(t)$, $u(t)$ for the Mf tide. Dotted line shows the regressing mean longitude N of the lunar node. During the Topex/Poseidon primary mission (1992–2002), the Mf signal strength was weaker than average, that is, $f < 1$. During the Jason-1 mission (2002–2008) it was stronger. The small higher frequency components in f, u arise from the first spectral line in Table A1, which brings in the second harmonic of the lunar perigee frequency.

In a tidal analysis of many years of data, as in our LOD analysis earlier, one may estimate all these lines individually. But in a shorter time-series, or even in a long time-series with significant noise, a combined analysis is recommended. The traditional method for a combined analysis (Doodson & Warburg 1941) exploits the fact that the tidal response at such close frequencies must have nearly identical admittances, that is, equal phases and amplitudes in the ratios of the potential in Table A1. The tidal oscillation of any constituent with amplitude A and phase lag G may then be written

$$f\,A\cos(\omega t + u - G) \tag{A1}$$

with amplitude modulation f and phase modulation u varying slowly relative to the tidal period $2\pi/\omega$, where ω is the frequency of the fundamental line. Doodson & Warburg (1941) tabulate formulae for evaluating f, u for the major lunar constituents, and for Mf they give

$$\begin{aligned} f &= 1.043 + 0.414\cos N, \\ u &= -23.7^\circ \sin N + 2.7^\circ \sin 2N - 0.4^\circ \sin 3N, \end{aligned} \tag{A2}$$

where N is the mean longitude of the moon's node ($N = -N'$ of Table A1). These expressions are usefully employed in many tidal analysis packages, but the extremely high precisions of the LOD tidal measurements warrant higher accuracy.

An oscillation of the Mf constituent can be written explicitly in terms of the four lines of Table A1 as

$$\begin{aligned} A_1\cos(2s - G) + A_2\cos(2s - 2p - G) + A_3\cos(2s + N' - G) \\ + \; A_4\cos(2s + 2N' - G), \end{aligned}$$

where the individual amplitudes A_n are assumed to be in the same ratios as the amplitudes V_0 of Table A1. By simple trigonometry, these four terms may be written in the form of eq. (A1) by solving the system

$$\begin{aligned} f\cos u &= 1 + 0.0432\cos 2p + 0.4145\cos N + 0.0387\cos 2N \\ f\sin u &= \quad -0.0432\sin 2p - 0.4145\sin N - 0.0387\sin 2N \end{aligned} \tag{A3}$$

for variables f, u.

To examine the benefit of the above formulae, we have partitioned the 1985–2003 LOD time-series into yearly subsets and subjected each year to independent tidal analysis. With the original Doodson–Warburg formula (A2), the scatter in the yearly Mf estimates has a standard deviation of 10.4 μs. Employing the system (A3) reduces the standard deviation to 4.0 μs. Such marked improvement is evident only because of the high precision of the LOD data. Formula (A2) is generally more than adequate for tidal analysis of noisier data, such as sea level.

The f, u variables for Mf are shown in Fig. A1 for the period 1975–2012. During the mid-1990s, we see that $f < 1$. During that period the two largest lines of Mf were out-of-phase, generating an Mf signal in tidal measurements which was smaller than average. In noisy measurements, such as those of sea level, the signal would have been more difficult to extract from background. For the 2003–2011 period, we have benefited from a stronger than average signal, allowing for more robust estimates of the fortnightly tide.